Carbon 96 (2016) 548–556

Contents lists available at ScienceDirect

Carbon

journal homepage: www.elsevier.com/locate/carbon

# Field-induced stretching and dynamic reorientation of functionalized multiwalled carbon nanotube aggregates in nematic liquid crystals

Weiwei Tie [a, b], Surjya Sarathi Bhattacharyya [b, c], Yange Zhang [a], Zhi Zheng [a], Tae Hoon Lee [d, e], Sang Won Lee [d, e], Tae Hyung Kim [b], Young Hee Lee [d, e, **], Seung Hee Lee [b, *]

[a] Key Laboratory of Micro-Nano Materials for Energy Storage and Conversion of Henan Province, Institute of Surface Micro and Nano Materials, School of Advanced Materials and Energy, Xuchang University, Henan 461000, China
[b] Applied Materials Institute for BIN Convergence, Department of BIN Fusion Technology and Graduate School of Printable and Flexible Electronics, Chonbuk National University, Jeonju, Jeonbuk 561-756, South Korea
[c] Asutosh College, 92, Shyamaprasad Mukherjee Road, Kolkata 700 026, West Bengal, India
[d] IBS Center for Integrated Nanostructure Physics, Institute for Basic Science, Sungkyunkwan University, Suwon 440-746, South Korea
[e] Department of Energy Science and Department of Physics, Sungkyunkwan University, Suwon 440-746, South Korea

ARTICLE INFO

*Article history:*
Received 27 May 2015
Received in revised form
22 September 2015
Accepted 25 September 2015
Available online 30 September 2015

ABSTRACT

Multiwalled carbon nanotubes (MWCNTs) exhibited distinct electrical stretching behavior in nematic liquid crystals (NLC) depending on nanotube surface state. We found that two different samples prepared by chemical functionalization (f-CNT) and physical grinding (g-CNT) revealed distinct field dependence from each other. The threshold stretching field was lower in the f-CNT aggregates than in g-CNT aggregates. This was attributed to polar functionality induced weakened van der Waals interaction in f-CNTs, which was confirmed in infrared (IR) and Raman spectroscopy. Dynamic reorientation of f-CNTs was observed under polarized optical microscopy where f-CNTs were found to follow orientation of NLC director. Uniformly aligned f-CNTs also exhibited selective light absorption in sufficiently long transient field off-state which could find potential applications in memory and modulator devices as well as the versatile functional composites.



## 1. Introduction

Nematic liquid crystals (NLCs) have attracted great attention in recent years for transferring their orientational order onto dispersed nanomaterials, especially highly anisotropic materials such as carbon nanotubes (CNTs) and graphene [1–6]. This hybrid LC-CNT represents a versatile composite system that has drawn a great deal of interests in fundamental and applied physics by exhibiting remarkable physical phenomena such as improvement in electrooptical characteristics of LC display [7–11], electromechanical memory effect [12–16], and homogeneous alignment of CNTs in different LC matrices for CNT-based device applications [17,18]. Nevertheless, CNTs tend to form aggregates in NLC (percolation limit 0.02–0.05 wt. % [15,19]) restricting the quantity of CNTs dispersing in NLC medium. Even at lower CNT concentration than percolation limit, CNTs cannot be often well dispersed in NLC matrix over macroscopic dimensions [17,20] due to strong van der Waals interaction between them, which greatly limits their practical applications.

Recently, electrically induced stretching behavior of CNT aggregates [21–25] has shown promising potential for macroscopic alignment of CNT aggregates along pre-determined direction, which would be favorable for large scale applications. In presence of electric field, the randomly oriented individual CNTs in aggregated form in LC matrix get unidirectional alignment along the field direction to minimize the induced dipolar energy due to their high aspect ratio and dielectrophoretic properties [26]. With further increasing field, the CNT aggregates could be stretched along the field direction above a critical field against van der Waals forces between CNTs bundles [25,26]. Extensive studies [21–25] to date

* Corresponding author.
** Corresponding author. IBS Center for Integrated Nanostructure Physics, Institute for Basic Science, Sungkyunkwan University, Suwon 440-746, South Korea.
*E-mail addresses:* leeyoung@skku.edu (Y.H. Lee), lsh1@chonbuk.ac.kr (S.H. Lee).

http://dx.doi.org/10.1016/j.carbon.2015.09.096
0008-6223/

have revealed field-dependent stretching of CNT aggregates related to the competition of applied field strength against van der Waals interaction between CNTs within aggregates. In general, functional groups on the CNT sidewalls will weaken van der Waals interaction between CNTs and promote the dispersion process [27,28]. The functional groups attached on the graphene-like surface of CNTs via various chemical reactions lead to reduce the inter CNT interaction caused either by electrostatic repulsion if they are charged or steric repulsion by creating space between the tubes that reduces the tube–tube van der Walls interaction. It is therefore imperative to further understand the effect of reduction of van der Waals interaction between tubes by the field-induced stretching behavior of CNT aggregates. Actually, a variety of modified CNTs through chemical and physical methods can be found in the literature [29–34]. Here, we use a common surface modification technique of chemical oxidative treatment for CNT covalent functionality [31]. This directly attaches carboxylic groups and other oxygen-bearing groups such as hydroxyl groups to ends and/or defect sites in the side-walls of CNTs while maintaining similar length distribution of CNTs compared to that with physical grinding treatment [20]. Therefore, the g-CNTs keep more graphitic structure integrity than f-CNTs. Thus these structural discrepancies will strongly affect van der Waals interaction between tubes [25]. Therefore, we expect a significant difference on the stretching behavior in self-assembled CNT aggregates due to the difference in respective structures from ground CNT to functionalized CNT samples. We demonstrate in the present paper the electric field-induced stretching behavior of functionalized CNT and ground CNT aggregates with respect to ac field strength and frequency and introduce the concept of stretching comparison of CNT aggregates for both types of samples. Transient field-off behavior of functionalized CNTs such as reorientation along NLC director field and selective light absorptions have also been discussed.

## 2. Experimental

The MWCNTs have been synthesized by catalytic chemical vapor deposition method using FeMoMgO catalyst prepared by a combustion method. The details of MWCNTs synthesis procedure have been reported elsewhere [20]. The transmission and scanning electron microscopic images of pristine MWCNTs are shown in fig. S1. The MWCNT sample was obtained in a powder form having the outer diameter in the range of 3–6 nm and lengths are ranged from 10 to 30 μm, which forms very large aggregates in NLC matrix. Therefore, the received MWCNTs have been shortened through two different cutting methods. The received MWCNT powders of 100 mg were stirred in 1 M sucrose solution for one hour. The sucrose-mediated CNT/sugar mixture was grinded in mortar for one hour. Here, sucrose was used as a surfactant in solution and also acted as a mediator to prevent the CNT damage from grinding process. After washing with deionized water several times, the sucrose was washed out and filtering, the CNTs are finally dried at 150 °C in order to obtain grinded MWCNTs, hereafter called g-CNT [20]. On the other hand, the received MWCNTs were functionalized by acid sonochemical oxidation process [31]. About 100 mg of the received MWCNT powder mixed with 50 ml of a 3:1 (v/v) mixture of concentrated $H_2SO_4$ (98%) and $HNO_3$ (68%) were placed in a 100 ml glass bottle and sonicated in a conventional ultra-sonic bath. Temperature (25–40 °C) and sonication power of the bath (100 W, 40 kHz) were kept mild for 8 h duration to minimize tube damage [29,34]. The supernatant was decanted after centrifugating at 3000 rpm for 30 min and was filtered by 0.2 μm anodic alumina membrane (Whatmann). Several cycles of centrifugation, washing in deionized water were performed until pH ~7, and also finally oven drying at 150 °C gave rise to MWCNT powder, hereafter called f-CNT. Either kind of CNTs (viz. g-CNT and f-CNT) was dispersed in ethanol by sonication for a quarter one hour.

The well-dispersed solution with CNT concentration of 0.167 g/ml were mixed with a negative dielectric anisotropic nematic LC ($\Delta\varepsilon = -4$) and nematic to isotropic transition temperature $T_{ni} = 75$ °C (MJ98468, Merck-Japan). Special care was taken to remove ethanol solvent using solvent evaporator kept at 70 °C. Either kind of the nanotubes in about $10^{-3}$ wt% concentration had been uniformly dispersed in the same NLC host in order to investigate and compare electric field-induced stretching behavior. Additionally, 0.08 wt% of f-CNTs was dispersed in the positive dielectric anisotropic nematic LC ($\Delta\varepsilon = +14$) viz. ZLI-4535, Merck-Japan; following above mentioned procedure in order to investigate the influence of NLC director over the dispersed CNTs.

Fourier Transformed Infrared (FT-IR) spectra was investigated with Perkin Elmer Spectrum-GX and Renishaw in Via and Raman spectroscopy was done with 532 nm laser excitation. The FT-IR and Raman analyses of g-CNTs and f-CNTs shown in Fig. 1 demonstrate that the f-CNTs attached with additional functional groups possessed different graphitic structural integrity from the g-CNTs.

Lengths and aggregate structures of f-CNTs and g-CNTs were examined by field emission-scanning electron microscopy (FE-SEM, JSM 700F, JEOL, Japan). Samples for SEM observations were prepared by mixing either kind of CNTs in 1,2-dichloroethane followed by 30 min sonication. Then, the supernatant was drop-dried on a clean glass. For the preparation of SEM samples for aggregates structure investigation, the abovementioned CNT-NLC mixtures after sonicating 10 min had been dropped onto transmission electron microscopy (TEM) grids (100 nm), pre-fixed on the filtration stage with filter paper. The samples collected over TEM grid had been examined by FE-SEM. The polarized transmission spectra of stretched CNTs in device had been measured by UV–Vis spectroscopy (Cary 5000 UV–vis–NIR spectrophotometer).

Average lengths of f-CNTs and g-CNTs were also measured by particle size analyzer (DLS-8000, Otsuka Electronics) for the dispersed solution containing 2 mg of f-CNTs or g-CNTs in 2 g of 1% sodium dodecyl sulfate (SDS) aqueous solution after sonication for 1 h.

In order to observe in-plane field-dependent behavior of the CNT aggregates, the interdigitated electrode pattern with an opaque aluminum metal was fabricated on bottom glass substrate. In order to achieve homogeneous alignment of NLC molecules, the alignment layer viz. SE-6514 (Nissan Chemicals) was spin-coated on both substrates and followed by baking at 200 °C for one hour. Then, rubbing process with rubbing angles of 0°, 10°, 45° with respect to in-plane field direction was applied. The interdigital electrodes were 10 μm wide maintaining an intra-electrode gap of 20 or 40 μm and the finally constructed cells were ~80 μm thick. The test cells were filled with the NLC-CNT mixture using a capillary action technique at room temperature. The textures of the test cells were observed by an optical microscope (Nikon DXM1200) while applying a sinusoidal field with adjusting frequency. All the experimental results shown in the present paper had been performed at room temperature (300 K) far from crystallization temperature of the NLC host.

## 3. Result and discussion

FT-IR spectroscopy has been carried out over g-CNTs and f-CNTs in order to identify the functionality of either kind as shown in Fig. 1(a). As described earlier, the f-CNTs were prepared through acid-sonochemical oxidation of pristine MWCNTs [31]; hence the effect of abovementioned oxidation process is scrutinized in the present investigation. The comparative analysis on FT-IR spectra clearly exhibits appearance of several new absorption peaks and

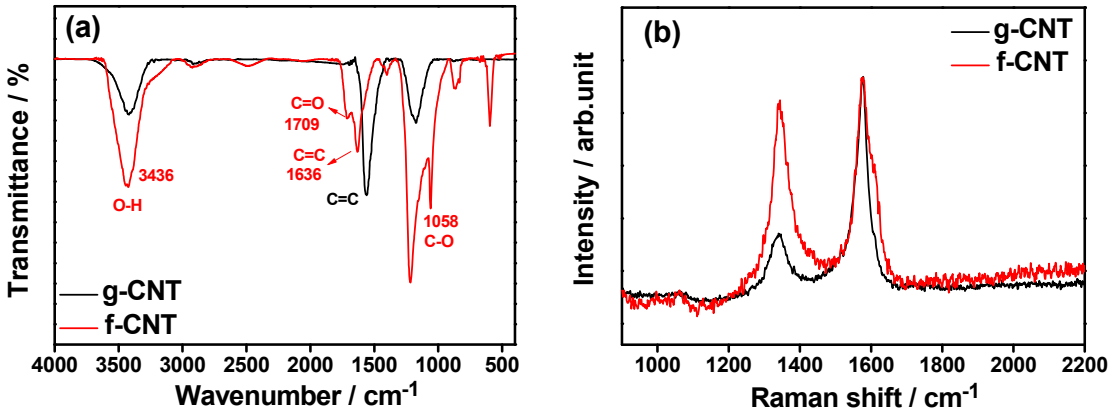


**Fig. 1.** FT-IR (a) and Raman (b) spectra of g-CNT and f-CNT. (A colour version of this figure can be viewed online).

bands for f-CNTs along with the characteristic peaks compared to that of g-CNTs sample. The new characteristic peak of functionalized CNTs appears at 1709 $cm^{-1}$, corresponding to stretching vibrations of carbonyl groups (C═O) present in carboxylic acids (−COOH) and at 1058 $cm^{-1}$ assigned to stretching vibrations of C−O. Absorption bands of CNT backbone appears at 2865−2960 $cm^{-1}$ (asymmetric and symmetric $CH_2$ stretching), 1562 $cm^{-1}$ (C═C stretching) for g-CNTs and 1636 $cm^{-1}$ (C═C stretching) for f-CNTs are found on both tubes. The results clearly indicate the carboxyl and other oxidized groups are successfully introduced onto CNT surface, in good agreements with earlier investigations [33].

Raman spectroscopic technique is utilized to investigate the disordered structure of the prepared CNTs for each kind. Fig. 1(b) shows the Raman spectra of g-CNTs and f-CNTs. The dominant Raman feature at around 1340 $cm^{-1}$ is amorphous or disordered non-graphitic carbon structure (D-band) and 1576 $cm^{-1}$ is in-plane tangential stretching of the carbon−carbon bonds (G-band) in graphene sheets. The existence of the band at around 1340 $cm^{-1}$ for both kinds implies that both grinding and acid-treatment process cause the cutting and the destruction of nanotubes. The $I_D/I_G$ ratios of f-CNTs and g-CNTs are 0.93 and 0.55, respectively. This indicates the chemical covalent modification with functionalization, which introduces large amount of non-graphitic carbon onto tube surface. This significantly affects the graphitic structural integrity of CNTs from $sp^2$ to $sp^3$ compared to that with physical grinding treatment. In other words, “structural integrity” is a measure of structural imperfection of nanotubes. Increasing of $I_D/I_G$ from 0.55 to 0.93 suggests that the treatment procedure applied to the nanotubes is quite destructive for these tubes. In these processes the tubes may lose their unique properties like quasi-metallic conductance along the tube axis.

Considering the differences in the CNT structure during the different modifying process, the dispersion in g-CNTs and f-CNTs is examined via SEM and DLS particle size analyzer. The corresponding results are shown in Fig. 2(a, b) and Fig. 2(c, d), respectively. Exemplary low resolution SEM images exhibit that lengths of g-CNTs and f-CNTs are around 290 nm with a certain size distribution. Despite the difficulty in precise measurement of the sizes of one dimensional nanotubes using light scattering analyzer, the relative size distribution has been roughly analyzed in well dispersed aqueous SDS solution [27]. The DLS confirms the most frequent appearance of CNTs of ~290 nm for both samples. Moreover, the lengths of g-CNTs are found to be distributed between 100 nm and 550 nm, which is more or less similar to f-CNTs lengths lying between 120 nm and 620 nm. The peaks at low sizes less than 50 nm are considered to be the CNT aggregate sizes. One can conjecture that the CNT aggregate size is reduced in f-CNTs.

The self-assembled g-CNT and f-CNT aggregates in NLC medium have been investigated through high magnification (×50,000) SEM, in order to reveal the structural differences if it exists, as shown in Fig. 3(a) and (b). From a comparative macroscopic view, it appears that the g-CNT aggregate shows more compact conformation than the f-CNT aggregate. Both aggregates appear to comprise nanometric cylindrical CNT bundles. The diameter distribution of cylindrical CNT bundles for g-CNTs and f-CNTs is shown in Fig. 3(c) and (d). The nanometric cylindrical constituents of g-CNT bundles show a distribution of diameters between 20 and 36 nm and those of f-CNT bundles are between 12 and 28 nm. Considering average outer diameter of individual CNTs ~5 nm and the dimension of g-CNT and f-CNT bundle ranging from 314 to 1027 and from 113 to 615, respectively, the number of g-CNTs and f-CNTs ranges from 62 to 200 and from 22 to 123 in each bundle. This indicates that the tube−tube interaction in f-CNT aggregate should be smaller due to presence of lesser number of tubes in each bundle and the bundle−bundle interaction in f-CNT aggregate seems to be small, evidenced by the sparse location of f-CNT bundles.

The micrometer-sized CNT aggregates dispersed in homogeneously aligned NLC medium in the mentioned cell geometry have been observed under optical microscope. Fig. 4 exhibits a representative stretching study of each CNT aggregate as a function of applied electric field strength at 10 kHz frequency. The optically measured lengths of the f-CNT aggregates along their respective axis of anisotropy in the off-field state are measured to be 1.5 and 3.6 μm and those for g-CNT counterpart are 1.8 and 2.4 μm, respectively.

The representative cases of f-CNT and g-CNT aggregate stretching phenomenon shown in Fig. 4 have been quantitatively depicted in Fig. 5 and Fig. 6. The relative variation in aggregate length ($\Delta l$) has been plotted as a function of applied in-plane field strength. Here,

$$\Delta l = l_E - l \tag{1}$$

where '$l_E$' and '$l$' represent the length of the aggregate for applied field strength '$E$' state and 'zero field' state. The distinct field-dependent behavior is obtained for both samples. The f-CNT aggregates with initial lengths of 1.5 and 3.6 μm are found to start stretching at a critical electric field ($E_{th}$) of 2.0 and 2.55 $V_{rms}/\mu m$, respectively, at a fixed frequency of 10 kHz. However, the stretching of g-CNT aggregates with initial lengths of 1.8 and 2.4 μm starts up to applied field strength as high as 4.0 $V_{rms}/\mu m$ at the same

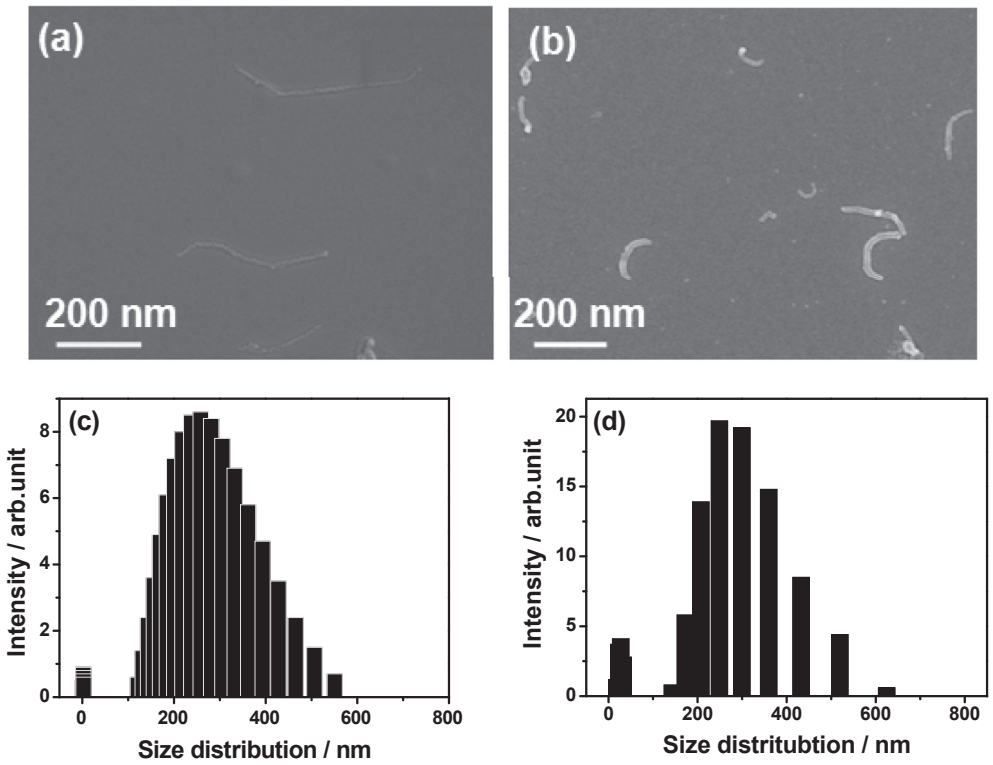


**Fig. 2.** Scanning electron microscopic images (a,b) and dynamic light scattering measurement (c,d) of g-CNT (a,c) and f-CNT (b,d).

frequency. The observed difference in stretching behavior has been investigated for hundreds of distinct aggregates and found to be reproducible.

Moreover, the aggregate-stretching with various frequencies has also been examined and their frequency induced stretching elongation ($\Delta l$) of representative cases for g-CNT and f-CNT aggregates has been depicted in Fig. 6, respectively. The stretching behavior has been observed within the wide frequency bandwidth (20 Hz–2 kHz) at a particular field of 2 $V_{rms}/\mu m$. Interestingly, we observe the significantly higher stretching elongation of f-CNT aggregates with initial lengths of 1.5 and 3.6 μm at each fixed frequency compared to that with initial length of 1.8 and 2.4 μm, although the stretching elongation for each kind decreases in response to frequency over the entirely investigated frequency range. Here, the translational movement of CNT aggregates between electrodes is observed in the frequency range of a few Hz to several tens Hz, which is driven by dielectrophoretic force and then followed by electric field-induced elongation as shown in Fig. 4.

The field-induced stretching behavior of the CNT aggregates has been reported in previous works [21–25], which can be explained by considering applied electric field-induced dipolar reordering of CNTs from random to a linear form. After applying electric field, the CNTs in the host medium experiences the force $\overrightarrow{F_{elec}}$ given by

$$\overrightarrow{F_{elec}} = -q\vec{E} + \vec{p}\cdot\nabla\vec{E} \tag{2}$$

where '$\vec{p}$' represents induced dipole moment and '$q$' represents the charge induced on the CNT aggregates in the presence of electric field '$\vec{E}$'. The first term '$q\vec{E}$' describes Coulombic interaction between charges induced in the particles and external field. The additional force term $(\vec{p}\cdot\nabla)\vec{E}$ arises from interaction between induced dipole moment of the particle and spatially inhomogeneous field. In the absence of electric field (E = 0), the CNTs are entangled in the form of bundles due to strong van der Waals interaction. Applied oscillatory electric field induces fast reversing the same and opposite charges over CNTs. With increasing field strength, the individual CNTs in bundles are aligned along the field direction to minimize the dipolar energy. Hence forth, above a certain field ($E > E_{th}$), Columbic interaction '$q\vec{E}$' overcomes van der Waals forces and CNT aggregates start to elongate along the field direction. With further increase of field ($E >> E_{th}$), individual CNTs will be forced to stretch out from the bundle and CNT are chained by inter CNT (dipole–dipole) interactions along the field direction when the Columbic force '$q\vec{E}$' further overcomes van der Waals force between CNTs. Hence, the stretching behaviors are related to competition between Columbic interaction which induced translation motions of charged CNTs and van der Walls interaction of CNTs in CNT aggregates. However, when the frequency increases, the dielectrophoretic force driven movement of CNT aggregates will decrease [28]. It has been reported in the abovementioned literature that CNTs can trap ions. The field induced translational motion of charged CNTs along the field direction decreases with increasing frequency as dipolar CNTs cannot follow fast reversing oscillatory electric field hence shows reduced elongation [28]. Therefore, with increasing frequency of applied field, the motion of charged CNTs in bundles will decrease along the field direction under the field Columbic force, and then lead to reduction of elongation of CNT aggregates. Hence, with increasing frequency the stretching behavior of MWCNTs aggregates in LC medium is reduced.

Considering self-assembled aggregate with comparable sizes and similar average length of nanotubes for each sample, the presence of oxygen-related functional groups in f-CNTs, which was evidenced by IR and Raman analysis, is mainly responsible for lower stretching threshold and higher frequency dependence in stretching behavior of f-CNT compared to those of g-CNT

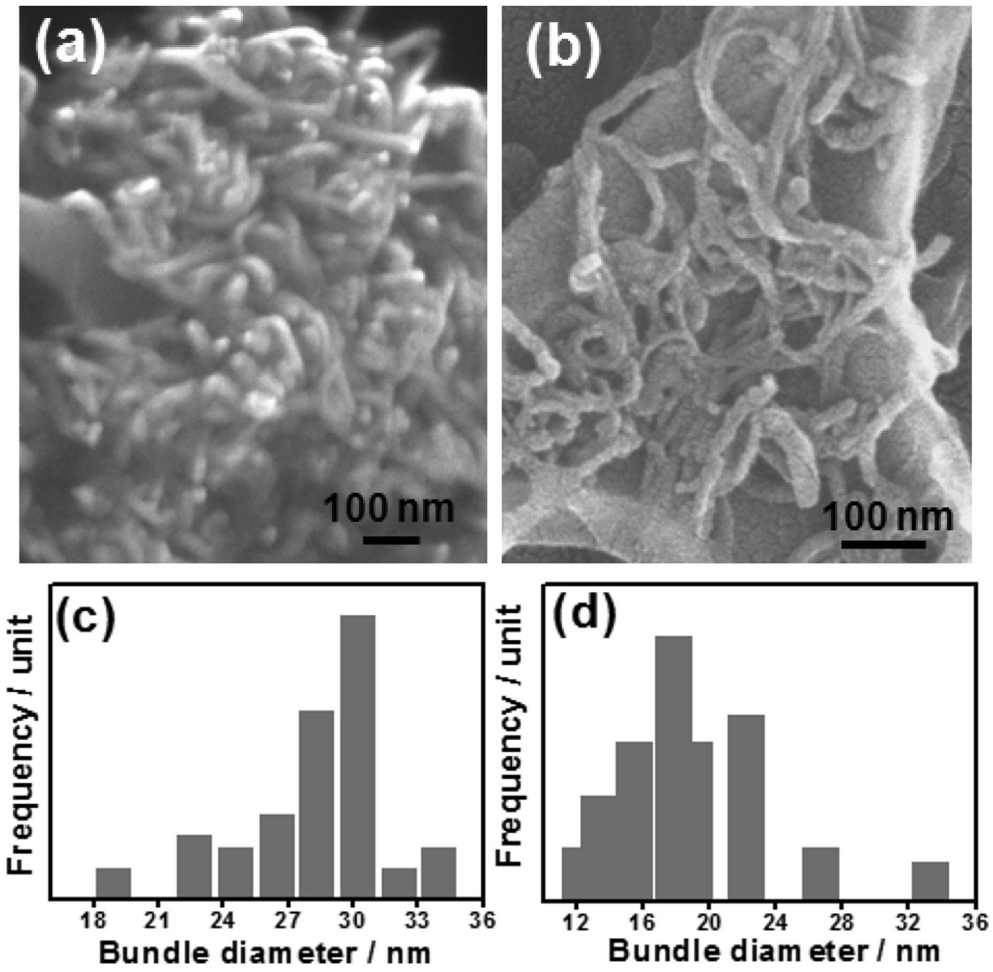


**Fig. 3.** Scanning electron microscopic images of initial state of (a) g-CNT and (b) f-CNT aggregate in NLC medium. (c) and (d) represents g-CNT and f-CNT bundle diameter distribution according to (a) and (b).

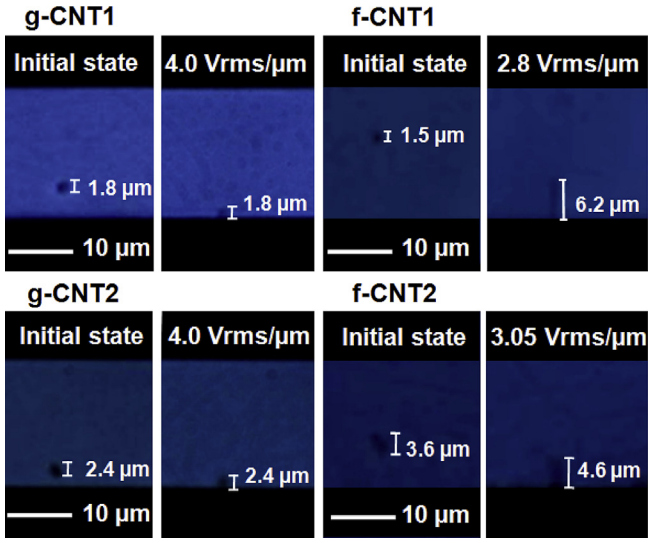


**Fig. 4.** In-plane field induced stretching of g-CNT and f-CNT aggregates as a function of electric field strength at 10 KHz. The sizes of g-CNT aggregates are 1.8 μm (case 1) and 2.4 μm (case 2), and the sizes of f-CNT aggregates are 1.5 μm (case 1) and 3.6 μm (case 2). (A colour version of this figure can be viewed online).

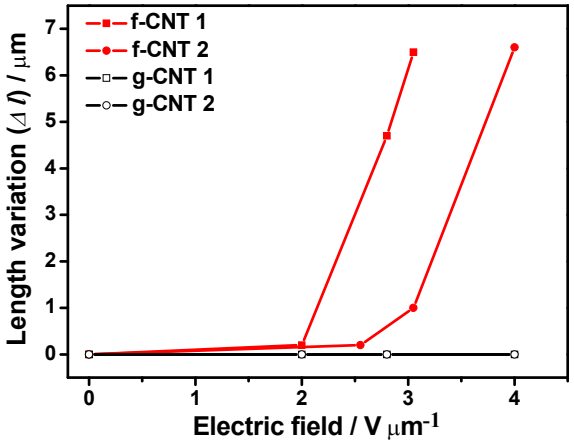


**Fig. 5.** Length variation of g-CNT and f-CNT aggregates as a function of electric field. (A colour version of this figure can be viewed online).

aggregates. Modification of f-CNT aggregates by acid-oxidation induces carboxyl and hydroxyl groups to form covalent bonds on the tube walls. Thus, on one hand, the charged f-CNTs with functionalized groups over tube walls will generate the electrostatic repulsion between nanotubes [35], opposing van der Walls

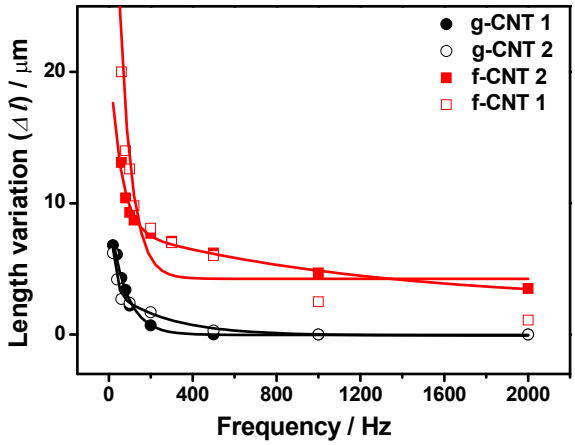


**Fig. 6.** In-plane field induced stretching of g-CNT and f-CNT aggregates as a function of frequency at field of 2 $V_{rms}/\mu m$. The sizes of g-CNT aggregates are 1.8 μm (case 1) and 2.4 μm (case 2), and the sizes of-CNT aggregates are 1.5 μm (case 1) and 3.6 μm (case 2). (A colour version of this figure can be viewed online).

interaction between f-CNTs; On the other hand, $sp^2$ hybridization responsible for π–π interaction of graphite surface is also reduced [30]. Consequently, π–π interaction between individual tubes in self-assembled f-CNTs remains considerably weak in aggregates. The previous analysis is proved by different tube–tube and inter-CNT bundle interactions though SEM analysis as reported in earlier section. Thus, due to weakened van der Waals interaction between tubes, with applying field ($E > E_{th}$), the f-CNTs in the aggregates can be easily aligned along field direction to minimize the dipolar energy and stretched to form chain by inter CNT (dipole–dipole) interaction along the field direction when the Columbic force '$q\vec{E}$' further overcomes van der Waals force between CNTs.

Fig. 7 exhibits the optical images of representative reorientation process of field-aligned f-CNT aggregates. Before applying field (a), the f-CNTs are randomly entangled into aggregates or aggregated in a macroscopic scale. After ac field treatment of 4 $V_{rms}/\mu m$ (b), CNTs are found to be uniformly orientated along the field direction. The field dependent orientation process of f-CNT aggregates in Fig. 7(a) with highlighted white area has been detailed in Fig. 7(e). The corresponding figures clearly depict the microsized f-CNT aggregates to be gradually aligned along field direction, while increasing the applied field strength. The randomly entangled f-CNT aggregates before field treatment are found to start aligning, followed by stretching above certain electric field in the range from 2.4 to 3.6 $V_{rms}/\mu m$, depending on self-assembled aggregate sizes. With further increasing field, the stretched CNT aggregates on both electrode sides start connecting to each other to form long straight

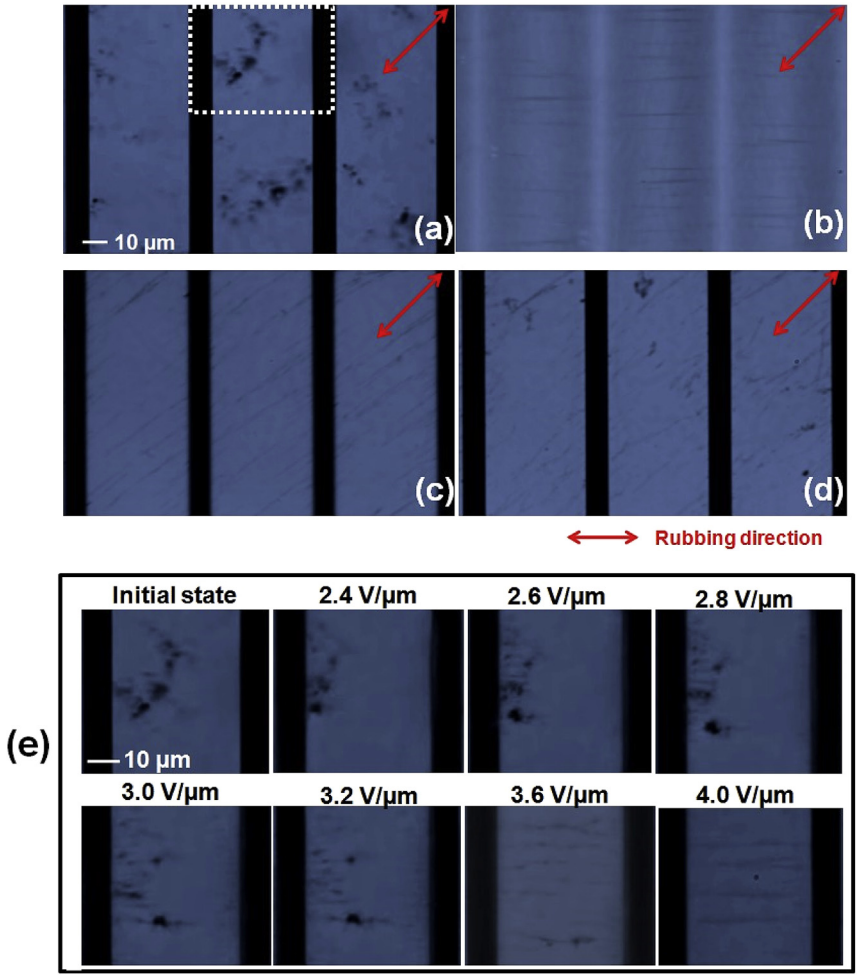


**Fig. 7.** Optical microphotographs of f-CNT aggregates at initial state (a) and field-on state of 4 Vrms/μm at 10 KHz (b). Figures (c) and (d) are optical microscopic images of fig. (b) at field off state below and above Tni. The red arrow indicates the rubbing direction with angle of 45° to the in-plane field direction. Fig. 7(e) is highlight area of Fig. 7(a) with white circle area exhibiting in-plane field induced orientation process of f-CNT aggregates as function of ac field strength. (A colour version of this figure can be viewed online).

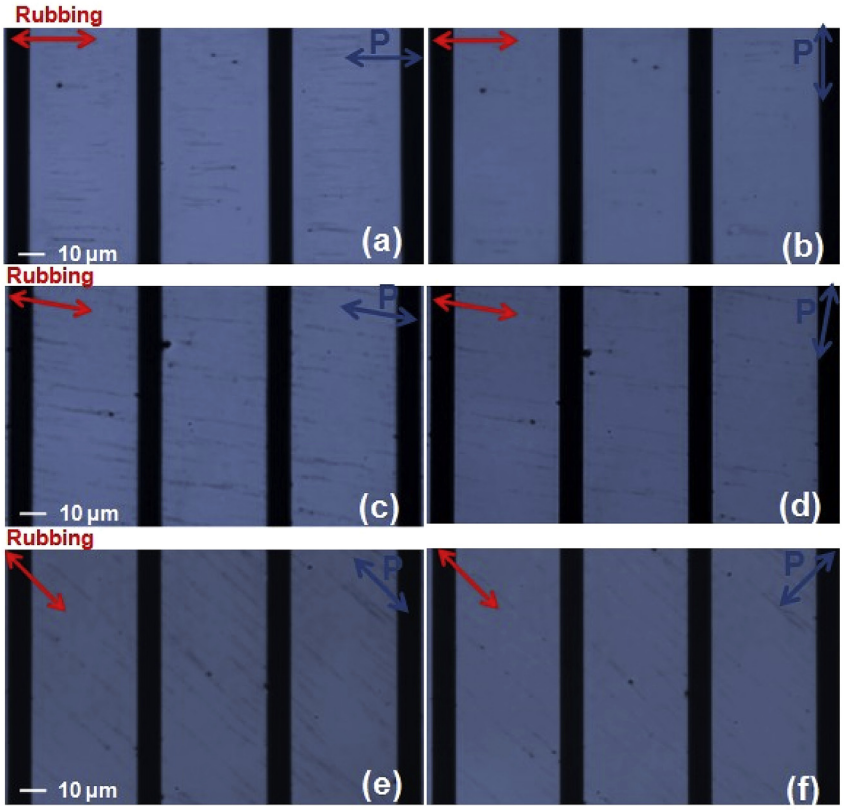


**Fig. 8.** Polarized optical microphotographs of aligned f-CNT aggregates with different substrates rubbed at (a) 0°, (b) 10° and (c) 45° angle with respect to the applied in-plane field direction. Here, polarized visible light incident on the cell with its electric vector parallel to the rubbing direction. Figures (b), (d), and (f) are optical microscopic images of same areas shown in figure (a), (c), and (e), respectively, when the polarized visible light propagates the cell with its electric vector perpendicular to the rubbing direction. The red and blue arrows indicate the rubbing direction and transmission axis of polarizer below bottom substrate, respectively. (A colour version of this figure can be viewed online).

bundles above the field of 3.6 $V_{rms}/\mu m$, while maintaining overall orientation along the direction of the electric field. Moreover, attractive connection of the stretched CNT aggregates along electrode direction leads to thicker bundles at a field of 4 $V_{rms}/\mu m$, which is mainly attributed to the increased electrophoretic movement along electrodes in response to the field strength. The thickness of f-CNT bundles varies in the range of hundreds of nanometers depending upon the applied field and frequency. Interestingly, after removal of applied field, the aligned CNT aggregates are not only found to remain elongated due to reduced van der Waals interaction between CNTs but also reoriented to 45° to follow NLC director field predetermined by the cell boundary condition, as shown in Fig. 7(c). The light intensity transmitted through random areas of electric field treated f-CNTs dispersed in NLCs in field off state has been determined in order to have a broader view over f-CNT aggregate relaxation process. The transmitted light intensity determined with the help of IMT *i*-solution software (Image & Microscope Technology Co., USA), through trial areas of test cells, remains invariant for as long as 20 h indicating the elongated f-CNTs continue to maintain the orientational order even after 20 h of field treatment. Note that the stretching behavior of said g-CNT sample has already been reported in previous papers [21,23], which shows instantaneous contraction after switching field off. This indicates NLCs surrounding the aligned f-CNT aggregates stabilize its alignment by elastic interaction with anisotropic LC host. Thus, reorientation of the aligned CNT aggregates is evident rather than individual CNTs responding to relaxation of NLCs. Similar self-organization and reorientation behavior is reminiscent in NLC-CNT system that theoretically and experimentally exhibits the alignment and reorientation of dispersed individual CNTs through NLCs caused by the coupling of the unperturbed LC director field to the anisotropic interfacial tension of the nanotubes in the nematic host fluid [2,3]. In order to verify the effect of NLC director field onto the reorientation of aligned CNT aggregates, the

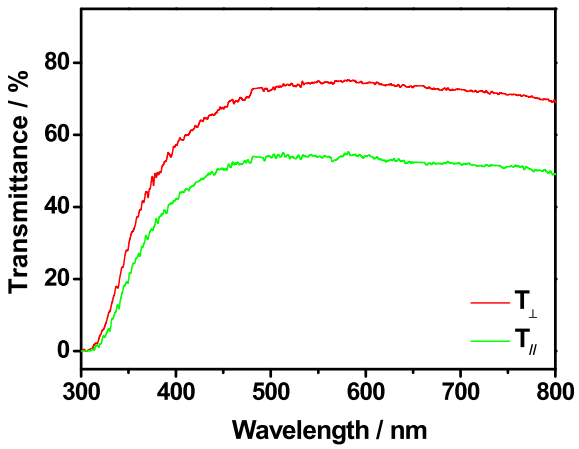


**Fig. 9.** Polarized transmission spectra of aligned f-CNT aggregates after stretching according to Fig. 8 (e, f). $T_{//}(T_{\perp})$ shows the transmittance for light linearly polarized parallel (perpendicular) to the stretching direction. (A colour version of this figure can be viewed online).

configuration of field-treated f-CNTs in NLC host has been investigated above $T_{ni}$ as shown in Fig. 7 (d). Re-aggregation tendency in f-CNTs in several areas indicates restoration of randomly entangled f-CNTs in the absence of anisotropic director field of NLC host.

Anisotropic light absorption properties of field aligned f-CNTs have been evaluated in field off-state under the polarized visible light. Fig. 8 shows polarized optical microscopic images of 4 Vrms/μm field treated f-CNT aggregates, while changing the polarization direction of an incident light parallel and perpendicular to initial LC director, which is a rubbing direction. Aggregates are found to stretch along the applied field (perpendicular to electrode direction) and reorient back to the rubbing direction viz. 0, 10, and 45° with respect to the applied in-plane field direction, which exactly follows NLC director as shown in Fig. 8 (a, b), (c, d) and (e, f) when releasing the applied electric field. Note that the transmission axis of polarizer is kept parallel to the rubbing direction (parallel to the stretched axis of the CNT aggregates) in figures (a, c, e), and kept perpendicular to the rubbing direction (perpendicular to the stretched axis of the CNT aggregates) in figures (b, d, f). The stretched f-CNTs are clearly visible as dark lines; however, the dark lines almost disappear, keeping only a few traces when polarizing axis of an incident light is rotated perpendicular to the rubbing direction. To further verify alignment of stretched f-CNTs with reorientation of LC director, the polarized transmission spectra of the device exhibited in Fig. 8 (e, f) has been reported in Fig. 9, where the transmission is remarkably lower for polarized visible light parallel to the LC director than for perpendicular. These results clearly indicate that the visible light with its electric vector ($E_{//}$) propagating along the long axis of the stretched CNT aggregate is absorbed by the CNT aggregate while the one ($E_{\perp}$) propagating along the short axis of the stretched CNT aggregate just passes through without absorption. Observed selective light absorption of aligned CNT aggregates is attributed to the anisotropic characteristics in the extinction coefficient ($\alpha$), in which the absorption of incident light with its electric vector along the long axis of CNT ($\alpha_{//}$) is different from that perpendicular to the long axis ($\alpha_{\perp}$), leading to the anisotropic light absorption [16,19,36,37]. This further confirms the orientation of aligned CNT aggregates remains stable via NLC director field during the reorientation process as discussed in the above section.

## 4. Conclusion

We have demonstrated the distinct in-plane field driven stretching behavior of MWCNT aggregates with different treatments of chemical oxidation (f-CNTs) and physical grinding (g-CNTs) dispersed in NLC host. The f-CNT aggregates reveal functionalized groups on the CNT walls. This gave rise to lower stretching threshold field and higher frequency dependent stretching ratio compared to that of g-CNT aggregates. The SEM observations exhibit that the g-CNT bundles consist of a larger number of individual CNTs than f-CNTs counterpart due to stronger van der Waals interaction between CNTs, and also confirms the different structural conformation of f-CNT and g-CNT aggregates with similar sizes in NLC medium. This structural difference in both CNT aggregates is mainly responsible for the above-mentioned distinct electrical stretching behavior of their aggregates. In addition, the control of orientation of f-CNTs with an electric field and nematic LC director field has been studied. The stretched f-CNTs align along electric field direction and reorient along NLC director in field off-state assisted by anisotropic elastic interaction via NLC director field. More importantly, the aligned f-CNTs absorb and transmit incident visible light when its electric vector of an incident light propagates parallel and perpendicular to long axis of the aligned f-CNTs, respectively. The alignment and reorientation behavior of field-treated CNTs in NLC opens up a new way of dynamically controlling CNT bundles or aggregates orientation rather than individual CNTs, which has potential applications for the realization of switchable electro-optic devices and multi-functional composites.

## Acknowledgments

This research was supported by Basic Science Research Program through the National Research Foundation of Korea (NRF) funded by the Ministry of Science, ICT & Future Planning (2014R1A4A1008140) and Polymer Materials Fusion Research Center. TWW also thanks to the financial support from the school scientific research fund of Xuchang University (2015-10).

## Appendix A. Supplementary data

Supplementary data related to this article can be found at http://dx.doi.org/10.1016/j.carbon.2015.09.096.

## References

[1] M.D. Lynch, D.L. Patrick, Organizing carbon nanotubes with liquid crystals, Nano Lett. 2 (2002) 1197–1201.
[2] I. Dierking, G. Scalia, P. Morales, D. Leclere, Aligning and reorienting carbon nanotubes with nematic liquid crystals, Adv. Mater. 16 (2004) 865–869.
[3] R. Basu, Effect of carbon nanotubes on the field-induced nematic switching, Appl. Phys. Lett. 103 (2013) 241906.
[4] R. Basu, G. Iannacchione, Orientational coupling enhancement in a carbon nanotube dispersed liquid crystal, Phys. Rev. E 81 (2010) 051705.
[5] Shin BG. NguyenVL, D.L. Duong, S.T. Kim, D. Perello, Y.J. Lim, et al., Seamless stitching of graphene domains on polished copper (111), Foil. Adv. Mater. 27 (2015) 1376–1382.
[6] W.W. Tie, S.S. Bhattacharyya, Y.J. Lim, S.W. Lee, T.H. Lee, S.H. Lee, et al., Dynamic electro-optic response of graphene/graphitic flakes in nematic liquid crystals, Opt. Express 21 (2013) 19867–19879.
[7] I.S. Baik, S.Y. Jeon, S.H. Lee, K.A. Park, S.H. Jeong, K.H. An, et al., Electrical-field effect on carbon nanotubes in a twisted nematic liquid crystal cell, Appl. Phys. Lett. 87 (2005) 263110.
[8] H.Y. Chen, W. Lee, N.A. Clark, Faster electro-optical response characteristics of a carbon-nanotube-nematic suspension, Appl. Phys. Lett. 90 (2007) 033510.
[9] S.Y. Jeon, S.H. Shin, S.J. Jeong, S.H. Lee, S.H. Jeong, Y.H. Lee, et al., Effects of carbon nanotubes on electro-optical characteristics of liquid crystal cell driven by in-plane field, Appl. Phys. Lett. 90 (2007) 121901.
[10] W. Lee, C. Wang, Y. Shih, Effects of carbon nanosolids on the electro-optical properties of a twisted nematic liquid-crystal host, Appl. Phys. Lett. 85 (2004) 513–515.
[11] H.Y. Chen, W. Lee, Suppression of field screening in nematic liquid crystals by carbon nanotubes, Appl. Phys. Lett. 88 (2006) 222105.
[12] R. Basu, G.S. Iannacchione, Nematic anchoring on carbon nanotubes, Appl. Phys. Lett. 95 (2009) 173113.
[13] R. Basu, G.S. Iannacchione, Dielectric hysteresis, relaxation dynamics, and nonvolatile memory effect in carbon nanotube dispersed liquid crystal, J. Appl. Phys. 106 (2009) 124312.
[14] L.A. Dolgov, N.I. Lebovka, O.V. Yaroshchuk, Effect of electrooptical memory in suspensions of carbon nanotubes in liquid crystals, Colloid J. 71 (2009) 603–611.
[15] L. Dolgov, O. Yaroshchuk, S. Tomylko, N. Lebovka, Electro-optical memory of a nematic liquid crystal doped by multi-walled carbon nanotubes, Condens. Matter Phys. 15 (2012) 1–8.
[16] O. Yaroshchuk, S. Tomylko, L. Gvozdovskyy, R. Yamaguchi, Cholesteric liquid crystal-carbon nanotube composites with photo-settable reversible and memory electro-optic modes, Appl. Opt. 52 (2013) E53–E59.
[17] J.P.F. Lagerwall, G. Scalia, Carbon nanotubes in liquid crystals, J. Mater. Chem. 18 (2008) 2890–2898.
[18] C. Zamora-Ledezma, C. Blanc, N. Puech, M. Maugey, C. Zakri, E. Anglaret, et al., Conductivity anisotropy of assembled and oriented carbon nanotubes, Phys. Rev. E 84 (2011) 062701.
[19] L.N. Lisetski, S.S. Minenko, V.V. Ponevchinsky, M.S. Soskin, A.I. Goncharuk, N.I. Lebovka, Mat.-wiss, U. Werkst. 42 (2011) 5–14.
[20] S.S. Bhattacharyya, G.H. Yang, W.W. Tie, Y.H. Lee, S.H. Lee, Electric-field induced elastic stretching of multiwalled carbon nanotube clusters: a realistic model, Phys. Chem. Chem. Phys. 13 (2011) 20435–20440.
[21] S.J. Jeong, K.A. Park, S.H. Jeong, H.J. Jeong, K.H. An, C.W. Nah, et al., Electroactive superelongation of carbon nanotube aggregates in liquid crystal medium, Nano Lett. 7 (2007) 2178–2182.
[22] P. Sureshkumar, A.K. Srivastava, S.J. Jeong, M.Y. Kim, E.M. Jo, S.H. Lee, et al., Anomalous electrokinetic dispersion of carbon nanotube clusters in liquid

crystal under electric field, J. Nanosci. Nanotechnol. 9 (2009) 4741–4746.
[23] B.G. Kang, Y.J. Lim, K.U. Jeong, K. Lee, Y.H. Lee, S.H. Lee, A tunable carbon nanotube polarizer, Nanotechnology 21 (2010) 405202.
[24] W.W. Tie, G.H. Yang, S.S. Bhattacharyya, Y.H. Lee, S.H. Lee, Electric-field-induced dispersion of multiwalled carbon nanotubes in nematic liquid crystal, J. Phys. Chem. C 115 (2011) 21652.
[25] W.W. Tie, S.S. Bhattacharyya, H.R. Park, J.H. Lee, S.W. Lee, T.H. Lee, et al., Comparative studies on field-induced stretching behavior of single-walled and multiwalled carbon nanotube clusters, Phys. Rev. E 90 (2014) 012508.
[26] H.W. Seo, C.S. Han, D.G. Choi, K.S. Kim, Y.H. Lee, Controlled assembly of single SWNTs bundle using dielectrophoresis, Microelectron. Eng. 81 (2005) 83–89.
[27] J.Y. Lee, J.S. Kim, K. Hyeok An, K. Lee, D.Y. Kim, D.J. Bae, et al., Electrophoretic and dynamic light scattering in evaluating dispersion and size distribution of single-walled carbon nanotubes, J. Nanosci. Nanotechnol. 5 (2005) 1045–1049.
[28] A.K. Srivastava, S.J. Jeong, M.H. Lee, S.H. Lee, S.H. Jeong, Y.H. Lee, Dielectrophoresis force driven dynamics of carbon nanotubes in liquid crystal medium, J. Appl. Phys. 102 (2007) 043503.
[29] K.L. Lu, R.M. Lago, Y.K. Chen, M.L.H. Green, P.J.F. Harris, S.C. Tsang, Mechanical damage of carbon nanotubes by ultrasound, Carbon 34 (1996) 814–816.
[30] L. Vaisman, H.D. Wagner, G. Marom, The role of surfactants in dispersion of carbon nanotubes, Adv. Colloid. Interface 128–130 (2006) 37–46.
[31] Y. Xing, L. Li, C.C. Chusuei, R.V. Hull, Sonochemical oxidation of multiwalled carbon nanotubes, Langmuir 21 (2005) 4185–4190.
[32] K. Balasubramanian, M. Burghard, Chemically functionalized carbon nanotubes, Small 1 (2005) 180–192.
[33] F. Avilés, J.V. Cauich-Rodríguez, L. Moo-Tah, A. May-Pat, R. Vargas-Coronado, Evaluation of mild acid oxidation treatments for MWCNT functionalization, Carbon 47 (2009) 2970–2975.
[34] J.H. Lee, T.W. Jeong, J.N. Heo, S.H. Park, D.H. Lee, J.B. Park, et al., Short carbon nanotubes produced by cryogenic crushing, Carbon 44 (2006) 2984–2989.
[35] K.A. Park, S.M. Lee, S.H. Lee, Y.H. Lee, Anchoring a liquid crystal molecule on a single-walled carbon nanotube, J. Phys. Chem. C 111 (2007) 1620–1624.
[36] R. Cervini, G.P. Simon, M. Ginic-Markovic, J.G. Matisons, C. Huynh, S. Hawkins, Aligned silane-treated MWCNT/liquid crystal polymer films, Nanotechnology 19 (2008) 175602.
[37] S. Shoji, H. Suzuki, R.P. Zaccaria, Z. Sekkat, S. Kawata, Optical polarizer made of uniaxially aligned short single-wall carbon nanotubes embedded in a polymer film, Phys. Rev. B 77 (2008) 153407.